JOURNAL OF SOLID STATE CHEMISTRY **128,** 30–37 (1997)
ARTICLE NO. SC967137

New Aurivillius-Related Phases in the Sb–(W, V)–O System: Structural Study and Properties

A. Ramirez,* R. Enjalbert,† J. M. Rojo,* and A. Castro*,[1]

*Instituto de Ciencia de Materiales de Madrid, CSIC, Cantoblanco, 28049 Madrid, Spain, and †Centre d'Elaboration de Matériaux et d'Etudes Structurales, CNRS, 29 rue Jeanne Marvig, B.P. 4347, 31055 Toulouse Cedex, France

Received May 9, 1996; in revised form September 6, 1996; accepted September 9, 1996

Two types of solid solutions ($Sb_2W_{1-x}V_xO_{6-x}$ with x up to 0.5 and $Sb_2W_{1-y}V_yO_{6-y/2}$ with y up to 0.4) have been obtained by substitution of W(VI) with V(IV) or V(V) in Sb_2WO_6. These materials have been studied by X-ray powder diffraction methods, showing a gradual evolution of the unit cell parameters according to the ionic radii of the different cations, as well as the appearance of oxygen vacancies in the network. Crystal growth of these phases has been carried out, and a single-crystal structure determination has been performed on a sample corresponding to the formula $Sb_2W_{0.75}V_{0.25}O_{5.75}$. This material crystallizes in the monoclinic system, space group $P2_1/a$, with unit cell parameters $a = 5.529(3)$, $b = 4.914(2)$, $c = 9.193(5)$ Å and $\beta = 96.04(4)^\circ$, and has been refined down to $R = 0.067$. The structure is related to the classical Aurivillius framework, being built up by alternating infinite [Sb–O] sheets with [(W,V)–O] layers, which include the oxygen vacancies. Impedance measurements were carried out on two representative $Sb_2W_{0.75}V_{0.25}O_{5.75}$ [V(IV)] and $Sb_2W_{0.75}V_{0.25}O_{5.875}$ [V(V)] samples. In both cases the electrical response is dominated by an electronic conductivity that is higher for the V(IV) ($Sb_2W_{0.75}V_{0.25}O_{5.75}$) compound.

INTRODUCTION

The mixed Sb_2VO_5 oxide with V(IV) has been prepared as a single crystal and its structure has been solved by X-ray diffraction methods (1). Sb_2VO_5 crystallizes in the monoclinic system, space group $C2/c$, and its framework is built up by $[Sb_2O_2]_n$ layers alternating with infinite sheets of VO_5 square pyramids sharing edges. This compound shows is affiliated with the orthorhombic form of Sb_2O_3 (2) and mainly with Sb_2WO_6 (3). In fact, Sb_2WO_6 crystallizes in the triclinic system, space group $P1$. Its crystal structure is built up by $[WO_4]_n$ layers of WO_6 octahedra sharing corners, as in the simplest Aurivillius phase Bi_2WO_6 (4–7), sandwiched by two $[Sb_2O_2]_n$ layers. Single crystals of this material are twinned at room temperature, according to the existence of domains, which disappear at high temperature, as observed by TEM and optical microscopy. This fact is correlated to ferroelastic (may be ferroelectric) behavior, with a transition range between 300 and 400°C (3).

Taking into account the similar structural frameworks and the interesting physical properties of Sb_2WO_6 and Bi_2WO_6 oxides (3, 8–12), some of the authors have previously prepared and studied two solid solutions of $Bi_{2-x}Sb_xWO_6$ composition; one of them is isostructural with the ferroelectric Bi_2WO_6 ($0 \leq x \leq 1.25$) and the other is isostructural with the ferroelastic Sb_2WO_6 ($1.5 < x \leq 2$) (13). Both types of structures keep the basic network of Aurivillius oxides, but the study of the structural evolution with x shows the progressive distortion of the Bi_2WO_6 prototype resulting in the Sb_2WO_6 structure.

Since the Sb_2WO_6 and Sb_2VO_5 oxides show a similar structural framework, the authors have attempted substitution of W(VI) with V(IV) or V(V) to obtain new Aurivillius-related materials with oxygen vacancies and/or cations with unfilled electronic levels [V(IV)]. In this way we have tried to enhance such electrical properties as ionic and/or electronic conductivity. This paper reports the existence of two solid solutions in the Sb_2VO_5–Sb_2WO_6–"$Sb_4V_2O_{11}$" ternary system together with a study of the structure and electrical properties of the new materials obtained.

EXPERIMENTAL

Synthesis

Powdered samples were prepared by solid state reactions from ground stoichiometric mixtures of analytical- grade Sb_2O_3, WO_3, VO_2 and V_2O_5 oxides. The mixtures were heated in sealed evacuated Vycor ampoules, to prevent the oxidation of Sb(III) to Sb(V) and of V(IV) to V(V), at increasing temperatures from 490 to 650°C for 24 h. After each thermal treatment the products were cooled to room temperature inside the furnace. Then, they were ground and examined by X-ray powder diffraction.

[1] To whom correspondence should be addressed.

0022-4596/97 $25.00

Single crystals of representative compositions were grown from melting stoichiometric mixtures of Sb_2O_3, WO_3, and VO_2 or V_2O_5 oxides. They were placed into ampoules which were sealed under vacuum and heated at 750°C for 24 h, then cooled to 400°C at $5°\ h^{-1}$ and to room temperature at $50°\ h^{-1}$. This protocol results in the formation of black or very dark platelet crystals of adequate size to be studied by X-ray single crystal diffraction methods.

Chemical Analysis

The W/V ratio was determined by chemical analysis from ground single crystals and was found to be in good agreement with the starting composition. Elemental analysis of W and V was done by emission ICP spectroscopy using a Perkin–Elmer Plasma 40.

Structural Studies

Powder X-ray diffraction patterns were recorded using graphite monochromatized Cu$K\alpha$ radiation, with a Siemens D-501 goniometer controlled by a DACO-MP computer, scanning from 5° to 110° (2θ), using steps of 0.05° (2θ) and counting 4 s for each step. Unit cell parameters of all single phases were refined by the Rietveld method (14), using the FULLPROF program (15).

The single-crystal quality and the crystal systems were first investigated on a precession camera. The diffraction data were collected using an Enraf–Nonius CAD4 diffractometer. Orientation matrix and cell parameters were obtained from least-squares refinements of setting angles of 25 reflections. Corrections of Lorentz polarization and empirical absorption (16) were applied to *hkl* data. Atomic scattering factors were corrected for anomalous dispersion (17). The calculations were performed with SHELX (18) and the drawings with ORTEP (19), run in a VFX/80 Alliant superminicomputer. The structure was determined by the Patterson method and subsequent Fourier and difference Fourier synthesis, and refined using full matrix least-squares calculations.

Conductivity Measurements

Electrical conductivity measurements were carried out by the complex impedance method in a 1174 Solartron frequency response analyzer. Pellets of approximately 10 mm diameter and 2-mm thickness were prepared and heated at 500°C for 12 h under vacuum. Platinum electrodes on the two faces of the pellets were obtained from a Pt (Engelhard 6082) paste that was heated at 200°C for 2 h and then at 500°C for 24 h under vacuum. The frequency range used was 10^{-1} to 10^5 Hz. The impedance measurements were carried out at different temperatures in the range 20–380°C with the pellet under a nitrogen flow.

RESULTS AND DISCUSSION

Sb_2WO_6–Sb_2VO_5 System

Nine samples of nominal composition $Sb_2W_{1-x}V_xO_{6-x}$ [V(IV)], with $x = 0$, 0.1, 0.25, 0.4, 0.5, 0.6, 0.75, 0.9, and 1, were prepared as microcrystalline powders. Compounds with the limits $x = 0$ (Sb_2WO_6) and $x = 1$ (Sb_2VO_5), which are well-characterized compounds, were also prepared for comparative purposes. The color of the $x = 0$ sample is dark green, whereas that of the $0 < x < 0.6$ phases is black. For $0.6 \leq x < 1$, the color evolves to green and, finally, for $x = 1$ the product becomes pale green.

Figure 1 shows the X-ray diffraction patterns of all the samples obtained. As can be seen, a solid solution exists for $0 \leq x < 0.6$, related to the structural type of Sb_2WO_6, while for $0.6 \leq x < 1$, a mixture of Sb_2WO_6 and Sb_2VO_5 oxide types appears to be present. This fact could not be improved by further variations in the reaction conditions.

To understand the structural evolution in the $Sb_2W_{1-x}V_xO_{6-x}$ solid solution, single crystals of two representative compositions, $x = 0.1$ and $x = 0.25$, were grown. Crystals of both phases were first studied by precession methods. $Sb_2W_{0.9}V_{0.1}O_{5.9}$ are always twinned crystals

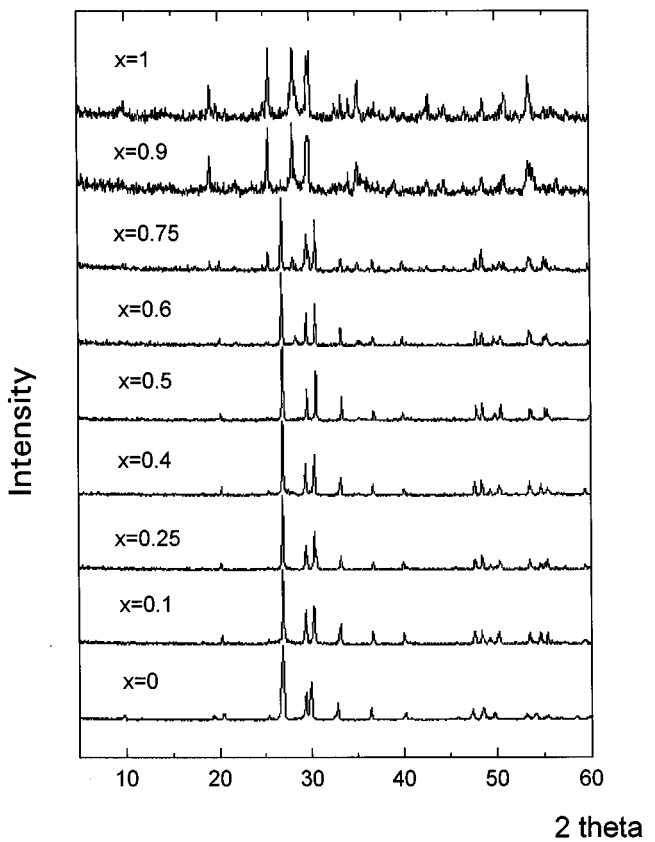

FIG. 1. X-ray diffraction patterns of $Sb_2W_{1-x}V_xO_{6-x}$ phases [V(IV)].

TABLE 1
Crystallographic Data for $Sb_2W_{0.75}V_{0.25}O_{5.75}$

Crystal data	
Crystal system	Monoclinic
Space group	$P2_1/a$
a (Å)	5.529(3)
b (Å)	4.914(2)
c (Å)	9.193(3)
β (°)	96.04(4)
V (Å^3)	248.4(2)
Z	2
Molecular weight	486.1
ρ calc (g cm^{-3})	6.50
μ (Mo$K\alpha$) (cm^{-1})	297
Morphology	Platelet
Color	Black
Dimensions (mm)	$0.15 \times 0.12 \times 0.018$
Data collection	
Temperature (°C)	20
Wavelength (Mo$K\alpha$) (Å)	0.71069
Monochromator	Graphite
Scan mode	ω–2θ
Scan width (°)	$0.90 + 0.35 \tan\theta$
Take-off angle (°)	3.8
Max Bragg angle (°)	35
T_{max}(s)	60
hkl ranges	$h\ 0 \rightarrow 8, k\ 0 \rightarrow 7, l - 14 \rightarrow 14$
Structure refinement	
Reflections collected	1264
Reflections unique measured	992
Reflections unique used $I \geq 3\sigma$ (I)	810
Parameters refined	43
Weighting	1
$R = \sum \|\|F_o\| - \|F_c\|\| / \sum \|F_o\|$	0.063
$R_w = [\sum w(\|F_o\| - \|F_c\|)^2 / \sum w F_o^2]^{1/2}$	0.069

TABLE 3
Selected Distances (Å) and Angles (°) for $Sb_2W_{0.75}V_{0.25}O_{5.75}$

Environmnet of W/V atom			
W/V–O1	$1.870(8) \times 2$ axial	O1–W/V–O1	180
–O2	$1.922(7) \times 2$ equatorial	O1–W/V–O2	$89.5(4) \times 2$
	$1.934(8) \times 2$		$89.5(5) \times 2$
			$90.5(5) \times 2$
			$91.5(4) \times 2$
		O2–W/V–O2	$87.8(3) \times 2$
			$92.2(3) \times 2$
			180×2
O1 ⋯ O2	from 2.66 to 2.71		
O2 ⋯ O2	from 2.67 to 2.78		
Environment of Sb atom			
Sb–O3[a]	1.978(8)	O3[a]–Sb–O3	90.4(2)
–O3	2.027(8)	–O1	88.3(3)
–O1	2.101(6)	–O3[b]	87.9(2)
		–O1[a]	69.1(3)
–O3[b]	2.404(8)	O3–Sb–O1	79.4(4)
–O1[a]	2.585(8)	–O3[b]	69.5(2)
		–O1[a]	149.0(3)
		O1–Sb–O3[b]	148.6(4)
		–O1[a]	77.0(4)
		O3[b]–Sb–O1[a]	129.8(3)
Sb–E	0.97		
O1 ⋯ O3	from 2.54 to 2.85		

[a] $\frac{1}{2} + x, \frac{1}{2} - y, z$.
[b] $1 - x, -y, 1 - z$.

showing a triclinic symmetry and unit cell parameters close to those of Sb_2WO_6 (ferroelastic material). The most interesting feature was observed for $Sb_2W_{0.75}V_{0.25}O_{5.75}$, whose Laue and precession diagrams showed that this material crystallizes in the monoclinic system and confirmed no twinning of all the tested crystals. The structure of $Sb_2W_{0.75}V_{0.25}O_{5.75}$ has been determined by single-crystal diffraction methods. Table 1 summarizes physical and crystallographic data together with the conditions of data collection. The final of fractional coordinates and equivalent isotropic thermal parameters are listed in Table 2. The selected bond distances and angles are listed in Table 3.

The general framework of $Sb_2W_{0.75}V_{0.25}O_{5.75}$ (Fig. 2a) keeps the layered arrangement of the Sb_2WO_6 (3) and Sb_2VO_5 (1) oxides, being built up by antimony– oxygen and tungsten/vanadium–oxygen infinite slabs parallel to the

TABLE 2
Final Atomic Parameters for $Sb_2W_{0.75}V_{0.25}O_{5.75}$

Atom	Site	x	y	z	Occupancy	U_{eq} (Å^2)[a]
W/V	2a	0	0	0	0.75/0.25	0.0131(4)
Sb	4e	0.6469(2)	0.0441(2)	0.3330(1)	1	0.0177(5)
O1	4e	0.513(2)	0.353(3)	0.188(1)	1	0.024(4)
O2	4e	0.718(2)	0.220(2)	0.944(1)	0.875	0.016(4)
O3	4e	0.365(2)	0.183(3)	0.436(1)	1	0.022(4)

[a] $U_{eq} = 1/3$ (trace u).

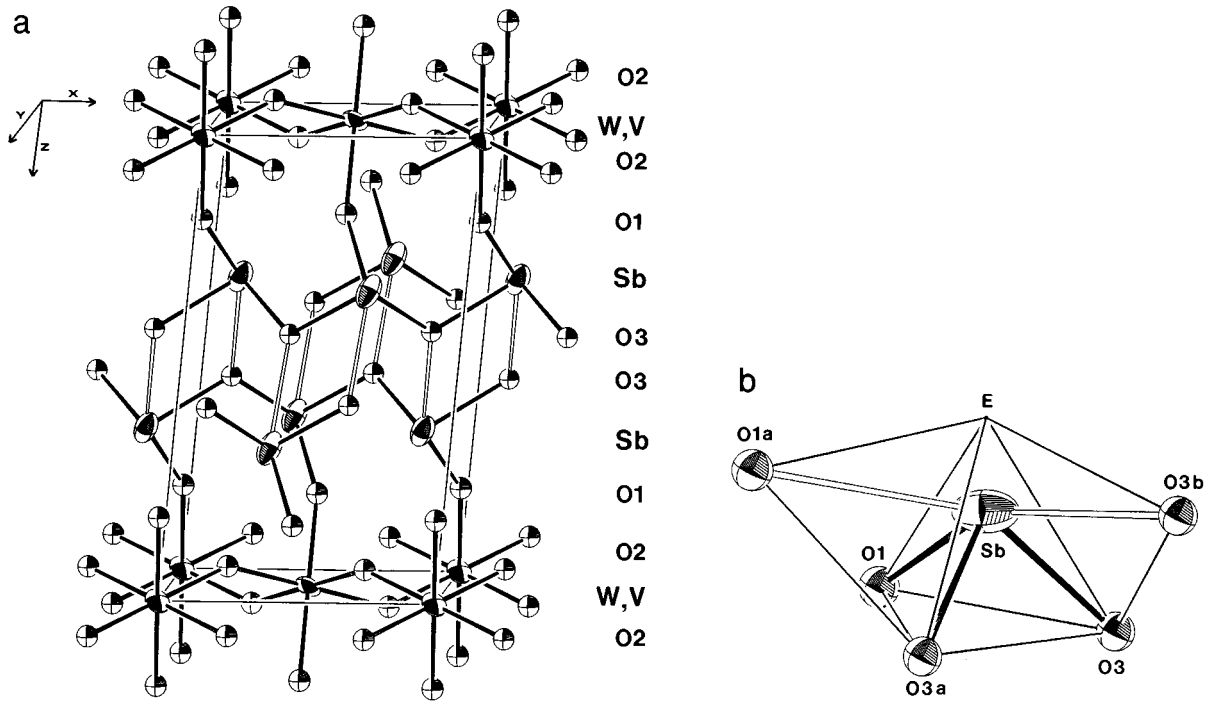

FIG. 2. (a) View of the crystal structure of $Sb_2W_{0.75}V_{0.25}O_{5.75}$. (b) Coordination polyhedron of antimony atoms (*E*, lone pair of electrons; symmetry code: $a \rightarrow \frac{1}{2} + x, \frac{1}{2} - y, z$; $b \rightarrow 1 - x, -y, 1 - z$).

(001) plane, which bind together along the [001] direction through weak Sb–O3 bonds.

The antimony atoms are coordinated to three oxygens at short distances, between 1.99 and 2.06 Å, two of its layer (O3) and the third (O1) the apices of the [W, V–O] layer, and to other two oxygens at longer distances: 2.40 Å, Sb–O3, and 2.59 Å, Sb–O1. The bond valence value obtained for antimony atoms taking into account only the shorter antimony–oxygen distances was to 2.44, whereas the other weak bonds must be considered to obtain the more realistic value of 2.92 (20, 21). This is a typical coordination of atoms possessing a stereoactive lone pair of electrons, such as Sb(III) (CN = 3 + 2). Thus, oxygen atoms and the lone pair (E) give rise to the bicapped tetrahedron shown in Fig. 2b. The position of E has been calculated following Galy *et al.* method (22).

The tungsten and/or vanadium atoms are octahedrally surrounded by oxygen atoms, sharing corners in the (001) plane, giving rise to the [(W, V)–O] layers. The interatomic W–O distances are in good agreement with those found in the limiting Sb_2WO_6 material (3); however, the coordination of W and/or V atoms can be also discussed in terms of bond valence theory (20, 21), taking into account that the mean valence of the metallic atoms in the tungsten/vanadium–oxygen layer is +5.50, in this oxide. The bond valence, $S = 0.75S_W + 0.25S_V$, calculated according to the composition, is 5.64 ($S_W = 6.10$, $S_V = 4.46$), giving rise to an apparent slight overbonding. The difference found between the expected and calculated values can be explained on the basis of the existence of oxygen vacancies in this layer, which must be formulated as $[(W, V)O_{3.75}]_n$, i.e., 6.25% of free oxygen positions. The existence of such vacancies suggests the change from octahedral to square pyramidal arrangements of anions around vanadium atoms. On the other hand, a residue of electron density of $4.6\,e\,Å^{-3}$, at coordinates $x = 0.076$, $y = 0.003$, and $z = -0.001$ appears on the final difference Fourier synthesis. This finding could reasonably represent the random distribution of both W and V atoms and their coordination polyhedra mainly in the [100] direction.

Contrary to Sb_2WO_6, $Sb_2W_{0.75}V_{0.25}O_{5.75}$ is a centric material at room temperature, that shows no evidence of triclinic distortion and ferroelastic behavior. Then, it is possible that substitutions of W(VI) with V(IV) in Sb_2WO_6 alter that property; a study of this is now in progress.

The unit cell parameters of five powdered single phases of $Sb_2W_{1-x}V_xO_{6-x}$ have been refined taking as structural models those determined by the single-crystal method: triclinic system, space group $P1$, for $x \leq 0.1$; and monoclinic system, space group $P2_1/a$, for $0.25 \leq x \leq 0.5$. For consistency, the parameters corresponding to $x = 0$ have also been measured. As can be observed in Table 4, the lattice constants clearly show continuous variation as a function of increasing V(IV) concentration, demonstrating that this

TABLE 4
Unit Cell Constants for the Phases of $Sb_2W_{1-x}V_xO_{6-x}$ Solid Solution

x	a (Å)	b (Å)	c (Å)	α (°)	β (°)	γ (°)	V (Å^3)
			Triclinic system, space group $P1$				
0	5.566(2)	4.948(2)	9.233(4)	90.12(3)	96.99(2)	90.24(3)	252.4(6)
0.1	5.556(2)	4.925(2)	9.229(4)	89.68(3)	96.50(3)	90.40(3)	250.9(6)
			Monoclinic system, space group $P2_1/a$				
0.25	5.538(1)	4.918(2)	9.209(3)	90	96.12(2)	90	249.4(4)
0.4	5.5069(9)	4.894(1)	9.166(2)	90	95.77(1)	90	245.8(3)
0.5	5.506(2)	4.884(2)	9.131(3)	90	95.25(2)	90	244.5(5)

system forms a solid solution. The decrease noted in a, b, and c parameters, as well as in the volume, with increasing x, from $x = 0$ to $x = 0.5$, is obviously related to substitution of V^{4+} cation for W^{6+}. Moreover, this decrease is greater than that expected from the difference of the effective ionic radii [$r(V^{4+}) = 0.58$ Å, $r(W^{6+}) = 0.60$ Å] (23) and can be explained by assuming the existence of oxygen vacancies in the network, related to the x value.

Sb_2WO_6–"$Sb_4V_2O_{11}$" System

Since substitutions for W(VI) in Sb_2WO_6 can be achieved with V(IV), the authors similarly doped with V(V), preparing materials of nominal composition $Sb_2W_{1-y}V_yO_{6-y/2}$. In this case, very dark powders were obtained for all $y > 0$ values. The X-ray diffraction patterns (Fig. 3) show the existence of single phases related to Sb_2WO_6 for $0 \le y \le 0.4$, similar to the above-described solid solution, whereas for $0.4 < y < 1$ a mixture of phases was detected; finally, when $y = 1$ (starting stoichiometry "$Sb_4V_2O_{11}$") only a rutile phase is observed, which could represent a member of the Sb(V)–V(III)–O family of nonstoichiometric rutile oxides (24–28). Its formation is due to a process of oxidation of Sb(III) to Sb(V) and reduction of V(V) to V(III). The formation of this very stable phase explains the small doping by V(V) in the Sb_2WO_6 phase, unlike that exhibited by V(IV).

Single crystals of several compositions for the solid solution $Sb_2W_{1-y}V_yO_{6-y/2}$ have been grown and studied by precession methods. In all cases the crystals are twinned and exhibit the characteristic triclinic symmetry of Sb_2WO_6 materials. The lattice constants for five single phases have been refined by X-ray powder diffraction methods, keeping the space group, $P1$, of Sb_2WO_6. As in the $Sb_2W_{1-x}V_xO_{6-x}$ solid solution, a decrease in all a, b, c and V unit cell parameters is observed (Table 5), which can easily be understood as due to the small ionic size of V^{5+} in comparison to W^{6+} [$r(V^{5+}) = 0.54$ Å] (23) and to the introduction of oxygen vacancies, probably into the [(W,V)–O] layers of the structure.

Sb_2VO_5–Sb_2WO_6–"$Sb_4V_2O_{11}$" Ternary System

To verify whether V(IV) and V(V) can coexist in the Sb_2WO_6 structure, different compositions in the ternary region shown in Fig. 4 have been investigated. For x and y values greater than the limits previously established in the solid solutions $Sb_2W_{1-x}V_xO_{6-x}$ and $Sb_2W_{1-y}V_yO_{6-y/2}$, 0.5 and 0.4, respectively, a mixture of rutile Sb_2VO_5- and Sb_2WO_6-type phases was always obtained, independent of

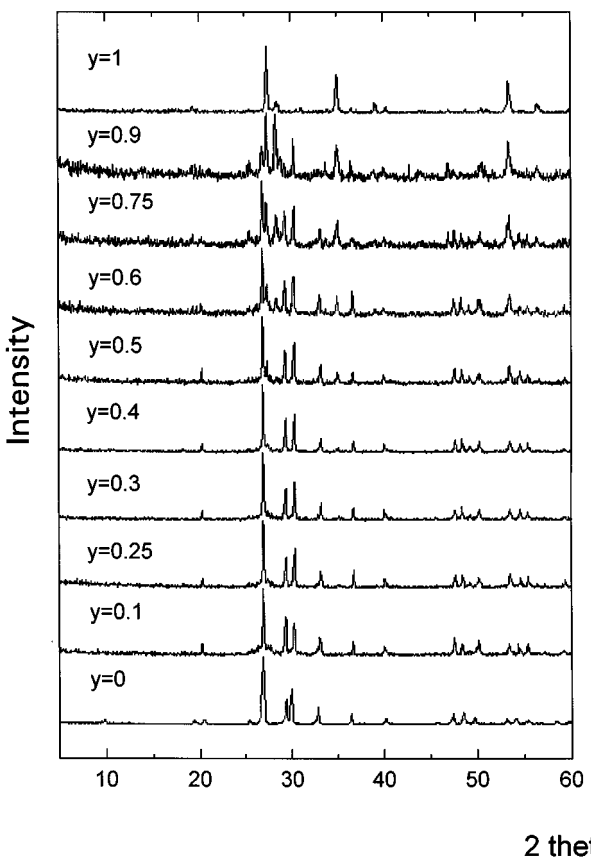

FIG. 3. X-ray diffraction patterns of $Sb_2W_{1-y}V_yO_{6-y/2}$ phases [V(V)].

TABLE 5
Lattice Parameters for the Phases of $Sb_2W_{1-y}V_yO_{6-y/2}$ Solid Solution (Triclinic System, Space Group *P*1)

y	a (Å)	b (Å)	c (Å)	α (°)	β (°)	γ (°)	V (Å^3)
0	5.566(2)	4.948(2)	9.233(4)	90.12(3)	96.99(2)	90.24(3)	252.4(6)
0.1	5.544(2)	4.924(3)	9.234(3)	90.12(3)	96.32(3)	90.46(2)	250.5(6)
0.25	5.532(2)	4.910(2)	9.222(3)	90.12(2)	96.08(2)	90.36(2)	249.0(5)
0.3	5.514(1)	4.899(1)	9.189(2)	90.02(2)	95.89(2)	90.23(2)	246.9(5)
0.4	5.504(1)	4.892(1)	9.176(2)	90.15(2)	95.86(1)	90.00(2)	245.8(3)

the starting compositions, although for both $x < 0.5$ and $y < 0.4$, apparent Sb_2WO_6 single phases are isolated.

Applying the crystal growth method established for the above solid solutions, an inhomogeneous preparation is obtained in every case. Some crystals belong to the triclinic system, whereas others belong to the monoclinic one. This may be due to the segregation of V(IV) and V(V) phases and not to the coexistence of both cations in the Sb_2WO_6 structural type.

Electrical Properties

The single crystals obtained in this work were of insufficient size for electrical measurements, which were carried out on pellets prepared following the procedure described under Experimental. The pellets were measured at different temperatures (20–380°C) under a nitrogen flow to avoid the oxidation of Sb(III) to Sb(V) and of V(IV) to V(V). The impedance plots (imaginary $-Z''$ vs real Z') of the $Sb_2W_{0.75}V_{0.25}O_{5.875}$ ($Sb_2W_{1-y}V_yO_{6-y/2}$, $y = 0.25$), obtained at the indicated temperatures, are shown in Fig. 5a. At 60°C an asymmetric arc is observed. It seems that the arc overlaps another small one in the high-frequency region. When the sample is heated at higher temperatures (140 and 380°C) the arcs disappear from the impedance plots. In addition, a spike, usually ascribed to blocking ion effects at the electrode surfaces, is not detected. The impedance plots of $Sb_2W_{0.75}V_{0.25}O_{5.75}$ ($Sb_2W_{1-x}V_xO_{6-x}$, $x = 0.25$), not shown in this paper, are similar to those of the $y = 0.25$ sample, but in this case only an arc, open at high frequencies, is observed.

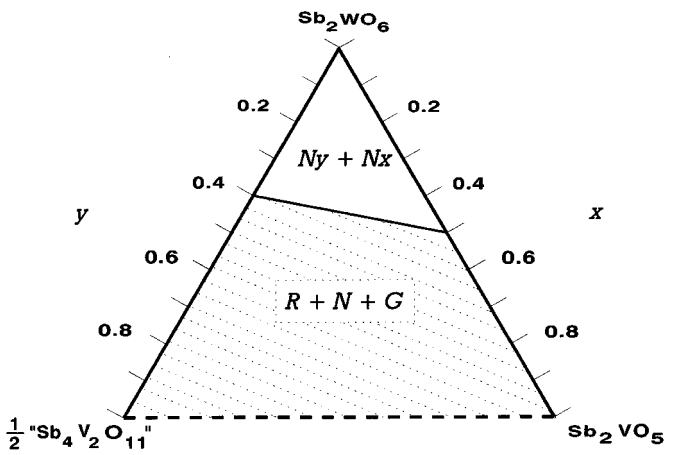

FIG. 4. Loci of solid solutions and mixture of phases in the Sb_2VO_5-Sb_2WO_6–"$Sb_4V_2O_{11}$" ternary system at 650°C: R, rutile-type phase; G, Sb_2VO_5 oxide; N, Sb_2WO_6 structural type; Nx, $Sb_2W_{1-x}V_xO_{6-x}$ solid solution (triclinic or monoclinic phases); Ny, $Sb_2W_{1-y}V_yO_{6-y/2}$ solid solution (triclinic phases).

The frequency dependence of the imaginary (ε'') and real (ε') parts of the permittivity in decimal log–log scale is shown in Figs. 5b and 5c, respectively. When the $y = 0.25$ sample is heated above 140°C, ε'' follows a linear dependence with slope -1 (solid line), whereas ε' shows a plateau. Both facts are well understood in terms of a true dc electronic conduction (29). An electronic conduction has also been reported in other Aurivillius compounds (30). For temperatures below 140°C, besides the behavior described for $\varepsilon''$and ε' in the low-frequency region, two new dependencies of those parameters in the high-frequency region are observed: ε' shows a dispersive regime, whereas ε'' seems to follow another linear dependence with lower slope. The high-frequency behavior of ε'' and ε' is associated with ac conductivity, probably related to diffusion of oxygen vacancies (31–36) according to the oxygen deficit of the [(W, V)–O] layers; however, the oxide ion conduction does not appreciably affect dc conductivity (low-frequency region) which is dominated by hopping electron conduction. This indicates that a portion of V is V(IV) in the $y = 0.25$ sample despite the majority of V(V). For the $x = 0.25$ sample, in which most of the V is V(IV), the electronic conduction is reinforced as deduced from plots of ε'' and ε' versus frequency (not shown in this paper). In this case the linear dependence of ε'' with slope -1 and the plateau of ε' are extended over a wider frequency region.

In both samples the dc conductivity was deduced from the impedance plots as follows: the resistance at each temperature was determined by the intersection of the impedance arcs with the real axis, then the dc values were calculated through the expression $(1/R)(h/s)$, where R is the resistance, h the thickness, and s the surface area of the

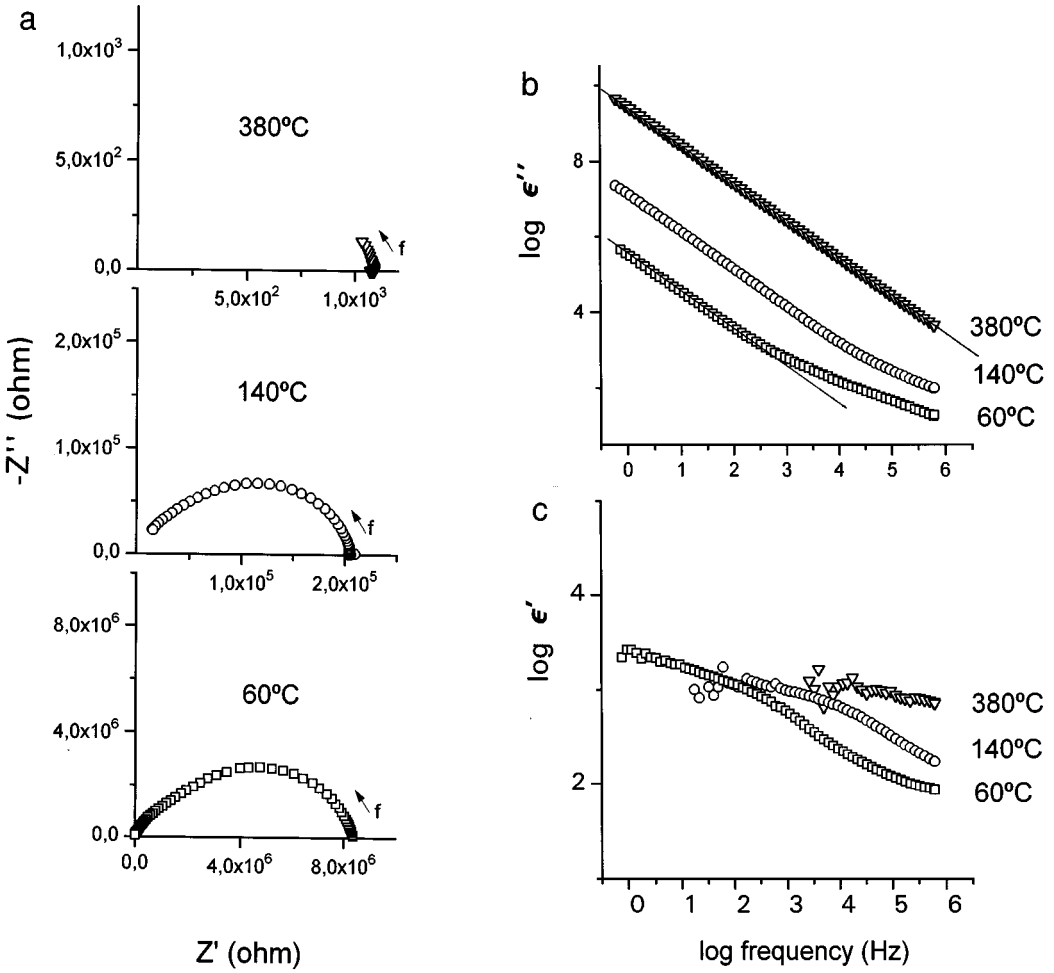

FIG. 5. Electrical measurements carried out on the $Sb_2W_{0.75}V_{0.25}O_{5.875}$ ($Sb_2W_{1-y}V_yO_{6-y/2}$, $y = 0.25$) sample. Impedance plots (imaginary vs real part) obtained at the indicated temperatures (a). Frequency dependence of the relative imaginary (b) and real (c) permittivity at three temperatures.

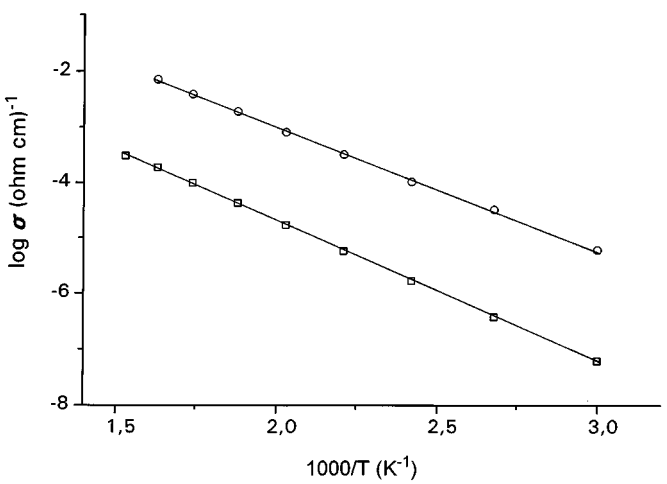

FIG. 6. Plot of $\log\sigma$ versus $1000/T$ for the $Sb_2W_{0.75}V_{0.25}O_{5.875}$ ($Sb_2W_{1-y}V_yO_{6-y/2}$, $y = 0.25$) (□) and $Sb_2W_{0.75}V_{0.25}O_{5.75}$ ($Sb_2W_{1-x}V_xO_{6-x}$, $x = 0.25$) (○) samples. The experimental data are well fitted by two Arrhenius equations.

pellet, respectively. Variation of the dc conductivity ($\log\sigma$) with inverse temperature ($1000/T$) for the $y = 0.25$ and $x = 0.25$ samples is shown in Fig. 6. The conductivity is higher for the $x = 0.25$ sample, in agreement with a higher content of V(IV). In addition, the experimental points are well fitted by two Arrhenius equations, $\sigma = \sigma_0 \exp(-E/K_BT)$, where σ_0 is a preexponential factor, E the activation energy, and K_B the Boltzmann constant. In that figure two straight lines are observed, being the E values 0.50 ± 0.01 and 0.44 ± 0.01 eV for the $y = 0.25$ and $x = 0.25$ samples, respectively. The activation energies found for both phases are close; however, these values are lower than those usually found for Aurivillius compounds in which conductivity is dominated by diffusion of oxide ions (30–32).

ACKNOWLEDGMENTS

The authors express their gratitude to DGICYT of Spain for financial support (Project PB92-1088). They also thank CNRS of France and CSIC

of Spain for the aid under a joint project. Prof. Dr. J. Galy is gratefully acknowledged for helpful discussions.

REFERENCES

1. B. Darriet, J. O. Bovin, and J. Galy, *J. Solid State Chem.* **19,** 205 (1976).
2. C. Svensson, *Acta Crytallogr. B* **30,** 458 (1974).
3. A. Castro, P. Millán, R. Enjalbert, E. Snöeck, and J. Galy, *Mater. Res. Bull.* **29,** 871 (1994).
4. B. Aurivillius, *Ark. Kemi.* **5,** 39 (1952).
5. R. W. Wolfe, R. E. Newnham, and M. I. Kay, *Solid State Commun.* **7,** 1797 (1969).
6. A. D. Rae, J. G. Thompson, and R. L. Withers, *Acta Crystallogr. B* **47,** 870 (1991).
7. K. S. Knight, *Miner. Mag.* **56,** 399 (1992).
8. H. W. Newkirk, P. Quadflieg, J. Liebertz, and A. Kockel, *Ferroelectrics* **4,** 51 (1972).
9. S. Yu. Stefanovich, and Yu. N. Venetsev, *Phys. Status Solidi A* **20,** 49 (1973).
10. I. G. Ismailzade, and F. A. Mirishli, *Kristallografiya* **14,** 738 (1970).
11. V. K. Yanovskii, V. I. Voronkova, A. L. Alexandrovskii, and V. A. D'Yakov, *Dokl. Akad. Nauk SSSR* **222,** 94 (1975).
12. V. I. Utkin, Yu. E. Roginskaya, V. I. Voronkova, V. K. Yanovskii, B. Sh. Galyamov, and Yu. N. Venetsev, *Phys. Status Solidi A* **59,** 75 (1980).
13. A. Castro, P. Millán, and R. Enjalbert, *Mater. Res. Bull.* **30**, 871 (1995).
14. H. M. Rietveld, *J. Appl. Crystallogr.* **2,** 65 (1969).
15. J. Rodríguez-Carvajal, "FULLPROF: A Programm for Rietveld and Pattern Matching Analysis." Abstracts of the Satellite Meeting of the XVth Congress of the International Union of Crystallography, Toulouse, France, 1990.
16. A. C. T. North, D. C. Phillips, and F. S. Mattews, *Acta Crystallogr. A* **24,** 351 (1968).
17. D. T. Cromer, and D. Liberman, "International Tables for X-Ray Crystallography." Vol. IV. Kynoch Press, Birmingham, UK, 1974.
18. G. Sheldrick, "SHELX-86: Program for Crystal Structure Determination." Oxford Univ. Press, Cambridge, UK, 1986.
19. C. K. Johson, "Ortep II Report ORNL 5138." Oak Ridge National Laboratory, Oak Ridge, TN, 1976.
20. I. D. Brown, *in* "Structure and Bonding in Crystals" (M. O'Keefe, and A. Navrotsky, Eds.). Wiley, New York, 1981.
21. I. D. Brown, and D. Altermatt, *Acta Crystallogr. B* **41,** 244 (1985).
22. J. Galy, G. Meunier, S. Andersson, and A. Åström, *J. Solid State Chem.* **13,** 142 (1975).
23. R. D. Shannon, *Acta Crystallogr. A* **32,** 751 (1976).
24. T. Birchall, and A. W. Sleight, *Inorg. Chem.* **15,** 868 (1976).
25. F. J. Berry, M. E. Brett, and W. R. Patterson, *J. Chem. Soc. Dalton Trans.*, 9 (1983).
26. S. Hansen, K. Ståhl, R. Nilsson, and A. Andersson, *J. Solid State Chem.* **102,** 340 (1993).
27. R. Enjalbert, M. Ewanje, J. Bonvoisin, and J. Galy, XX^{èmes} Journées d'Etudes des Equilibres entre Phases, Bordeaux, France, 1994.
28. A. Landa-Cánovas, J. Nilsson, S. Hansen, K. Ståhl, and A. Andersson, *J. Solid State Chem.* **116,** 369 (1995).
29. A. K. Jonscher, "Dielectric Relaxation in Solids." Chelsea Dielectrics Press, London, 1983.
30. K. R. Kendall, C. Navas, J. K. Thomas, and H. C. zur Loye, *Chem. Mater.* **8,** 642 (1996).
31. K. R. Kendall, J. K. Thomas, and H. C. zur Loye, *Chem. Mater.* **7,** 50 (1995).
32. K. R. Kendall, J. K. Thomas, and H. C. zur Loye, *Solid State Ionics* **70–71,** 221 (1994).
33. K. R. Kendall, J. K. Thomas, and H. C. zur Loye, *Solid State Ionics* **70–71,** 225 (1994).
34. R. N. Vannier, G. Mairesse, F. Abraham, and G. Nowogrocki, *Solid State Ionics* **70–71,** 248 (1994).
35. E. Pernot, M. Anne, M. Bacmann, P. Strobel, J. Fouletier, R. N. Vannier, G. Mairesse, F. Abraham, and G. Nowogrocki, *Solid State Ionics* **70–71,** 259, (1994).
36. A. Q. Pham, M. Puri, J. F. DiCarlo, and A. J. Jacobson, *Solid State Ionics* **72,** 309 (1994).